Journal of Materials Research and Technology 39 (2025) 5922–5936

Contents lists available at ScienceDirect

Journal of Materials Research and Technology

journal homepage: www.elsevier.com/locate/jmrt

Application of artificial neural networks in the development of elastomeric composite formulations with recovered carbon black from end–of–life tires

Jeferson Shiguemi Mukuno [a], Marcos Alves dos Santos [a], Gabriel Deltrejo Ribeiro [a], Dener da Silva Souza [a], Erivaldo Antônio da Silva [b], Leandro Ferreira Pinto [a], Henrique Pina Cardim [a], Michael Jones da Silva [a], Flávio Camargo Cabrera [a], Guilherme Pina Cardim [a], Carlos Toshiyuki Hiranobe [a], Renivaldo José dos Santos [a,*]

[a] *Postgraduate Program in Materials Science and Technology (POSMAT), School of Engineering and Sciences (FEC), São Paulo State University (UNESP), Avenida dos Barrageiros, 1881, Primavera, 19272-100, Rosana, São Paulo, Brazil*

[b] *Department of Cartographic and Surveying Engineering, School of Science and Technology (FCT), São Paulo State University (UNESP), Presidente Prudente Campus, Rua Roberto Simonsen, 305, 19060-900, Presidente Prudente, SP, Brazil*

ARTICLE INFO

Keywords:
Polybutadiene rubber
Recovered carbon black
Artificial neural networks
Properties prediction
Sustainable materials

ABSTRACT

In 2023, global tire production reached 2.3 billion units. After use, end-of-life tires pose a major environmental challenge due to their high resistance to degradation and the pollutant potential of vulcanization reagents. Tire pyrolysis has emerged as a sustainable alternative, generating gases, high-calorific-value oils, and recovered carbon black (rCB), which can be applied as a filler in elastomeric compounds. Although rCB exhibits properties similar to virgin carbon black (CB), variations in the composition of original tires compromise standardization and the mechanical performance of resulting composites. Numerous studies aim to enhance rCB performance using empirical trial-and-error approaches that require significant time, material, skilled labor, and energy. To optimize this process, this study proposes the use of artificial neural networks (ANNs) to predict the rheometric and mechanical properties of rCB-filled elastomeric composites prior to their fabrication, thereby reducing cost and minimizing unnecessary waste generation. Polybutadiene (BR) composites were prepared with rCB contents ranging from 0 to 50 phr. Experimental data were used to train nine ANNs to predict optimal cure time (t_{90}), hardness, density, abrasion resistance, crosslink density, tensile strength at break, elongation at break, and tear force and displacement at tear. The networks were trained using the Levenberg-Marquardt algorithm with Bayesian regularization. Predictions showed low error margins compared to experimental validation, confirming the accuracy of the models. The use of ANNs proved to be a reliable and efficient tool for the sustainable development of rCB-filled elastomeric composites, improving the vulcanization process and promoting resource optimization in the formulation of rubber materials.

1. Introduction

In 2023, global tire production reached 2.29 billion units [1], with 67 % manufactured in Asia and Oceania, 18 % in Europe, the Middle East, and Africa, and 15 % in South, Central, and North America [2]. Tires that are used, discarded, or no longer desired are classified as end-of-life tires (ELTs) [3–5].

According to data from the European Tyre & Rubber Manufacturers' Association [6] and the World Business Council for Sustainable Development [7], the global generation of ELTs reached approximately 31 million tons in 2023. China remained the leading producer, accounting for around 12.6 million tons (40.6 %), followed by the United States, with approximately 4.1 million tons (13.2 %). Together, these two countries were responsible for more than half of the ELTs generated worldwide. The remaining volume was distributed among regions such as the European Union (10.8 %), India (8.7 %), and other countries in Asia, Africa, and Latin America.

ELTs pose a significant environmental concern due to their complex composition, which includes carbon black, elastomeric compounds, steel wires, fibers, and various other organic and inorganic substances [8]. Approximately 60–65 % of a tire's weight consists of elastomers, 25–35 % is carbon black, 6–9 % comprises organic additives, 3–9 %

* Corresponding author.
E-mail address: renivaldo.santos@unesp.br (R.J. dos Santos).

https://doi.org/10.1016/j.jmrt.2025.10.196
Received 6 July 2025; Received in revised form 13 October 2025; Accepted 13 October 2025
Available online 25 October 2025

consists of inorganic additives, around 19 % is steel, and the remainder includes accelerators and fillers added during the manufacturing process [9–11].

These components can be recovered, provided that the solid waste is properly managed and directed to an appropriate destination, thereby making the process more sustainable. Among the most commonly applied treatments for tire waste are incineration and landfilling; however, these methods contribute significantly to environmental issues, such as the release of toxic emissions, greenhouse gases, and leachates [12].

As alternative disposal strategies for end-of-life tires, recovery, incorporation as aggregate, and pyrolysis are considered more economical and environmentally sustainable compared to landfilling. In the recovery process, the covalently crosslinked rubber structure can be disrupted, along with partial breakdown of polymer chains, through the combined application of thermal, mechanical, and chemical energy. The recovered rubber then becomes reprocessable and can be reshaped and revulcanized into new products.

The incorporation of rubber waste as an aggregate in cementitious mixtures for additive manufacturing also represents a viable route, in which rubber powder from end-of-life tires is used to replace sand in alkali-activated composites for 3D-printed construction materials, offering a sustainable alternative to conventional Portland cement-based concrete, known for its high CO_2 emissions [13].

In the pyrolysis process, tire waste is subjected to heating at temperatures ranging from 400 to 700 °C in an inert gas atmosphere (i.e., in the absence of oxygen), resulting in the production of activated carbon, recovered carbon black (rCB), pyrolytic oil, and pyrolytic gas. The rCB obtained through this method offers the advantage of lower cost and enables the sustainable reuse of solid residues that would otherwise impose a greater environmental burden.

Despite continuous improvements in production techniques, rCB still exhibits variability in its composition due to its source, as differences in tire properties can influence both the characteristics of the rCB and the final properties of the product in which it is applied [14]. These variations stem from differences in the formulation and manufacturing methods of tire compounds, which include component mixing, compounding, molding, and vulcanization.

Each elastomer has a specific set of properties that determines its suitability for a given application. Among synthetic rubbers, only polybutadiene rubber (BR) produces vulcanizates with elasticity and heat resistance superior to those of natural rubber (NR), indicating lower hysteresis and greater abrasion resistance and flexibility at low temperatures [15,16].

Currently, the research and development of vulcanized elastomers largely rely on a trial-and-error methodology, which demands substantial time and material resources. When specific mechanical properties such as hardness, tear resistance, or reduced curing time are required, multiple experimental iterations are typically performed to attain the desired performance. This practice often results in the generation of waste that is not always properly managed, alongside increased energy consumption and research-related expenses. The implementation of computational tools capable of predicting such properties offers the potential to considerably reduce material usage, time, and energy demands.

Since the mechanical and rheological properties of rubber compounds are influenced by multiple factors, including formulation and processing methods, the development of a computational system capable of managing numerous potentially interdependent variables while providing accurate predictions is essential. This requirement is consistent with the capabilities of artificial neural networks (ANNs), which have been increasingly applied in such predictive simulations. Due to their tolerance to outliers, ANNs can generalize the behavior of complex phenomena based on datasets, even identifying implicit patterns not directly evident in the training data [17,18]. ANNs establish and approximate input-output relationships by analyzing the training dataset, without depending on the complexity or scale of the problem [19].

ANNs are computational models inspired by the human brain, composed of multiple layers of interconnected artificial neurons [20]. The first layer is the input layer, where each neuron represents a specific type of information. This is followed by one or more hidden layers, consisting of artificial neurons interconnected with one another. During the training process, each connection is assigned a specific relevance (or weight), and each neuron is associated with a mathematical activation function, which allows the output of each neuron to be weighted accordingly. Each neuron in the hidden layer receives data from the preceding layer, applies its respective weight to each input, processes the information, and generates an output that is propagated through the network, influencing the subsequent neurons' responses [21]. Finally, an output layer produces the results of the network's computation.

ANNs can be applied across a wide range of fields, including natural language processing, pattern recognition, complex systems modeling, time series analysis, and functional prediction, due to their capacity for generalization and tolerance to anomalous or noisy input data [22]. They are particularly effective in approximating relationships between variables derived from experimental measurements in systems for which mathematical modeling is limited or infeasible [23].

With the aim of demonstrating the applicability of ANNs to elastomer research, Xiang (2014) [24], developed a study employing ANNs to predict the tensile fatigue resistance of natural rubber (NR) composites filled with carbon black (CB). The input dataset encompassed both mechanical parameters, including tensile strength at 100 %, tensile strength at break, and elongation at break, and viscoelastic characteristics, represented by tan δ at 7 % strain. The model achieved an average prediction accuracy of 97.3 %, highlighting the potential of ANNs to capture complex material behaviors. Similarly, Zhao et al. (2019) [25], proposed an ANN model to characterize the hysteretic behavior of magnetorheological elastomer (MRE) vibration isolators. This model demonstrated high predictive accuracy, effectively reproducing the nonlinear responses of MRE isolators under diverse excitation conditions. Collectively, these studies illustrate the effectiveness of ANNs in modeling intricate elastomer properties, supporting their use as a reliable predictive tool in polymer and elastomer engineering.

Based on these findings, it is reasonable to state that ANNs can be effectively employed as computational models for predicting the properties of rubber composites, thereby reducing the need for extensive laboratory testing. In this context, the present study focused on applying ANNs to predict nine data points related to seven rheological and mechanical properties of BR composites containing rCB. For each target output, an individual ANN was structured and trained, enabling the user to input the proportion of rCB relative to BR, and subsequently receive predictions for the remaining properties.

Using programming tools, the nine artificial neural networks (ANNs) were integrated into a computational application capable of accurately predicting the values of nine properties for each formulation. This strategy enhances both the safety and efficiency of the resulting products, while conserving energy and raw materials by reducing or potentially eliminating the reliance on traditional trial-and-error methods. Moreover, it contributes to minimizing rubber waste generation, shortens research time, and promotes the sustainable use of material resources through the application of recovered carbon black (rCB) derived from end-of-life truck tires.

2. Materials and methods

2.1. Materials

In this study, SABIC® 4610 BR was used, with a Mooney viscosity of 46 MU (ASTM D1646), a maximum volatile content of 0.5 %, and a maximum ash content of 0.25 % (ASTM D5667). The filler employed was PX-300 rCB, produced by Polimix Ambiental through the pyrolysis

of end-of-life truck tires. PX-300 rCB exhibits an iodine absorption value ranging from 70 to 89 g/kg (ASTM D1510), an oil absorption value between 75 and 90 cm^3/100 g (ASTM D2414), and a bulk density of 300–350 kg/m^3 (ASTM D1513).

The activators used were analytical-grade zinc oxide (ZnO), supplied by LABSYNTH, with a minimum purity of 99 %, and pure stearic acid ($C_{18}H_{36}O_2$) from the same supplier, with a melting point between 55 and 61 °C and an acid number ranging from 200 to 210. The plasticizer employed was polyethylene glycol (PEG) 4000 U S P., manufactured by Oxiteno. The curing agent was insoluble sulfur (non-oil treated), supplied by Êxodo Científica, with a minimum purity of 99.5 %, a melting point of 110–119.5 °C, a maximum ash content of 0.2 %, a maximum acidity of 0.1 %, and a maximum moisture content of 1 %. As accelerators, dibenzothiazole disulfide (MBTS) and tetramethylthiuram disulfide (TMTD) were used, both supplied by Basile Química Ltda.

After the rheological and mechanical tests were conducted, the resulting data were used to train the ANNs, which were developed and integrated using MATLAB 2024b, along with its Deep Learning Toolbox (v.23.2) and Statistics and Machine Learning Toolbox (v.23.2).

2.2. Preparation of composites

The composites were prepared using an open two-roll mill manufactured by Veiga, model V-MA-320, with a friction ratio of 1.25:1, in accordance with ASTM D3182-21a [26]. The formulation is presented in Table 1 in parts per hundred rubber (phr). Initially, the BR was mixed for 5 min to temporarily reduce its elasticity through partial polymer chain scission, thereby enhancing its plasticity and lowering compound viscosity to facilitate the incorporation of the activators (zinc oxide and stearic acid, which react to form zinc stearate), the plasticizer (PEG 4000), and the filler (rCB), until a homogeneous blend was obtained. Following this step, the compound was rested to ensure the complete formation of zinc stearate.

The mixture was then returned to the open mill for the addition of sulfur and the accelerators MBTS and TMTD, initiating the acceleration phase. Twelve specimens were prepared for each of the six formulations, totaling 72 samples, which were subjected to rheometric testing.

Once the t_{90} of each formulation was determined, test specimens for hardness, density, and abrasion resistance tests were prepared, as well as vulcanized rubber sheets according to ASTM D3182-21a [23]. These sheets were subsequently used to produce dumbbell-shaped specimens for tensile testing, in accordance with ASTM D412-16(2020) [27], and type C specimens for tear resistance testing, following ASTM D624-00 (2020) [28].

All test specimens and rubber sheets were vulcanized using a hydraulic press (Mastermac, model Vulcan 400/20-1) and a mold made of 1010/1020 steel, under a temperature of 160 °C and a pressure of 3 MPa, for the t_{90} curing time specific to each formulation. Once vulcanized, the rubber sheets (dimensions 150 × 150 × 2 mm) were cut into test specimens by shear using steel cutting dies and a manual hydraulic press.

Table 1
Formulations of BR-rCB composites (in phr).

Component	0 phr[d]	10 phr[d]	20 phr[d]	30 phr[d]	40 phr[d]	50 phr[d]
BR	100	100	100	100	100	100
Zinc oxide	4	4	4	4	4	4
Stearic acid	2	2	2	2	2	2
rCB	0	10	20	30	40	50
PEG 4000[a]	2	2	2	2	2	2
Sulfur	1,8	1,8	1,8	1,8	1,8	1,8
MBTS[b]	1,2	1,2	1,2	1,2	1,2	1,2
TMTD[c]	0,6	0,6	0,6	0,6	0,6	0,6

[a] polyethylene glycol.
[b] dibenzothiazole disulfide.
[c] tetramethylthiuram disulfide.
[d] The formulations were designated according to their filler loading (expressed in phr).

2.3. Characterization methods

2.3.1. Rheometric properties

The vulcanization parameters were determined from curing curves obtained using an oscillating disk rheometer (ODR) operating at a 1° arc and a temperature of 160 °C, in accordance with ASTM D2084-19a [29], using a TEAM Solutions rheometer (Teametro model). During the test, an axial oscillation was applied to the sample while the torque modulus was recorded over time, enabling the determination of the following parameters: minimum torque (M_L), maximum torque (M_H), scorch time (t_{S1}) and optimum vulcanization time (t_{90}).

2.3.2. Degree of filler dispersion in the polymeric matrix

The degree of filler dispersion (L) refers to an indicator that represents how uniformly the rCB particles are distributed within the polymeric matrix. A good dispersion is a determinant factor for the optimal performance of rubber. In rheometry testing, better dispersion generally leads to higher torque values and changes in other rheometric properties, as the rCB particles interact more effectively with the rubber matrix and resist deformation. It is possible to qualitatively evaluate the degree of filler dispersion indirectly by using the relationship between M_H and M_L [30], as shown in Equation (1):

$$L = \eta_r - m_r = \frac{M_{Lc}}{M_{Lg}} - \frac{M_{Hc}}{M_{Hg}} \quad (1)$$

Where:
L = degree of filler dispersion in the polymer matrix
η_r = minimum torque with rCB/minimum torque without rCB
m_r = maximum torque with rCB/maximum torque without rCB
M_{Lc} = minimum torque of the formulation with rCB
M_{Lg} = minimum torque of the formulation without rCB
M_{Hc} = maximum torque of the formulation with rCB
M_{Hg} = maximum torque of the formulation without rCB

2.3.3. Relative density test

The density of the rubber compositions was determined using the hydrostatic method, in accordance with ASTM D297-21 [31], which considers the mass of the specimen in air and the mass of the specimen suspended and fully immersed in a liquid of known density. The measured masses were applied in Equation (2):

$$\rho = \frac{\rho_L * m_A}{m_A - m_B} \quad (2)$$

Onde:
ρ = density of the specimen (g/cm^3)
ρ_L = density of ethanol at the analysis temperature (g/cm^3)
m_A = mass of the specimen in air (g)
m_B = mass of the specimen in liquid (g)

2.3.4. Crosslink density determination test by swelling in organic solvent

The crosslink density of the rubber composites was determined using the swelling technique. For this purpose, samples with a mass of approximately 0.25 ± 0.01 g were prepared and immersed in toluene for 5 days. After this period, the samples were removed, gently wiped to eliminate excess solvent, and weighed. Subsequently, the samples were placed in an oven at 85 °C for 24 h and weighed again.

The measured values of the sample mass before swelling, the mass after swelling, and the mass of retained solvent after drying were used to calculate the volume fraction of swollen rubber (V_B), and subsequently, the crosslink density (v), by applying Equation (3), developed by Flory and Rehner [32], which incorporates the Flory-Huggins interaction parameter χ [33] and the densities of both the rubber sample and the

solvent:

$$\nu = -\left(\frac{\ln(1-V_B)+V_B+\chi\cdot(V_B)^2}{\rho_B\cdot V_0\cdot\left(V_B^{\frac{1}{3}}-\frac{V_B}{2}\right)}\right) \quad (3)$$

Where:

ν = crosslink density (mol/cm^3)

V_B = volume fraction of swollen rubber, determined from swelling-induced weight gain (cm^3)

χ = Flory-Huggins interaction parameter

ρ_B = density of the rubber (g/cm^3)

V_0 = molar volume of the solvent (cm^3/mol)

2.3.5. Shore A hardness test

Shore A hardness was determined in accordance with ASTM D2240-15 [34]. This method consists of pressing an indenter into the surface of the test specimen, with the measured value being inversely proportional to the penetration depth; in other words, greater penetration indicates lower hardness. The Shore A scale is directly related to the elastic modulus of the material, such that higher Shore A values correspond to increased hardness and, consequently, greater material stiffness [35].

2.3.6. Abrasion resistance test

Abrasion resistance tests were conducted according to ASTM D5963-10 [36], using a Maqtest constant-rotation roller abrasimeter operating at a frequency of 40 cycles per minute. The cylinder has a diameter of 150 mm and an abrasion path length of 40 m. The lateral displacement of the specimen per one full rotation of the cylinder is 4.2 mm, and the force applied by the specimen onto the cylinder is 5.0 N. The inclination of the specimen holder's axis center relative to the vertical is 3°.

The specimen was clamped in a variable-diameter grip and subjected to a combined movement consisting of cylinder rotation, specimen translation over the cylinder, and compression against the abrasive paper. At the end of the cycle, the specimen was weighed again, and using these data, the abrasion loss was calculated according to Equation (4):

$$AL = \frac{(m_0 - m_1)\cdot S_0}{(\rho\cdot S)} \quad (4)$$

Where:

AL = abrasion loss (mm^3/40 m)

m_0 = mass before abrasion (mg)

m_1 = mass after abrasion (mg)

S_0 = theoretical abrasive index of the sandpaper on standard rubber (200 ± 20 mg)

S = actual abrasive index of the sandpaper on the rubber (mg)

ρ = composite density (mg/mm^3)

2.3.7. Tensile and tear resistance test

Tensile and tear resistance tests were conducted according to ASTM D412-16 [24], using type A (dumbbell-shaped) specimens, and ASTM D624-00 [25], using type C (right-angled) specimens, respectively. Twelve samples were prepared for each of the six formulations for both tests. The experiments were performed on a Biopdi universal testing machine equipped with an internal strain transducer, a 5 kN load cell, and a crosshead speed of 500 mm/min.

2.3.8. Artificial neural networks

ANNs operate by analyzing datasets through an iterative process of adjusting and storing synaptic weights assigned to each connection between neurons, thereby establishing dependency relationships between the input and output variables of the modeled system [16,37].

The operation of an ANN involves three fundamental stages: defining the network type, structuring the topology, and the learning (training) phase. The choice of network type depends on the nature of the problem to be modeled. For instance, feedforward neural networks (FNNs) are used for supervised tasks with independent and stationary data; convolutional neural networks (CNNs) are particularly effective in computer vision and image processing problems; whereas recurrent neural networks (RNNs) are more suitable for sequential data, such as time series or natural language [17,38].

During the structuring phase, the network topology is defined, which includes: the number of neurons in the input layer (related to the number of independent variables), the number of hidden layers and their respective neurons, the output layer, and the type of connections between neurons. Each connection is assigned a weight that determines its relative importance in the information propagation process. Furthermore, the activation function of each neuron is defined, responsible for introducing nonlinearity into the model. Functions such as ReLU (Rectified Linear Unit), sigmoid, or hyperbolic tangent are frequently employed, depending on the application type [34,39].

The learning phase corresponds to the period during which the network is trained using a labeled dataset (supervised learning) via optimization algorithms such as gradient descent or Levenberg-Marquardt. At each iteration, the connection weights are adjusted based on errors calculated from the difference between the predicted output and the desired output. The knowledge acquired by the network throughout training is represented by the final synaptic weight values [18,40]. If the network does not achieve satisfactory performance, strategies such as increasing the network depth (more hidden layers), increasing the width (more neurons per layer), or employing regularization techniques (e.g., dropout or Bayesian regularization) and alternative training functions may be used to improve generalization and reduce prediction error [35,41].

The application of ANNs for predicting mechanical properties of elastomeric compounds based on data obtained from laboratory tests offers advantages such as the nonlinearity of activation functions in hidden layer neurons, the capacity to relate input data to output without the need to specify a particular function, adaptability to the training data, and ease of implementation relative to the complexity of the ANN structure that can be generated [42].

However, it is important to highlight the need to address the challenge of selecting the optimal number of neurons in the hidden layer, as well as choosing the best set of input variables. Since there is no standard method for these selections, a loss in the model's generalization capacity may occur, as human intervention is always necessary to judge the most appropriate variables to apply [15].

Thus, through an empirical process, each ANN applied in this study was created by determining the number of neurons in the input layer, hidden layers, and output layer, as well as the number of hidden layers and the training function to be used, as presented in Table 2. Once the

Table 2
Architecture of created and trained ANNs.

ANN	Input layer	1st hidden layer	2nd hidden layer	3rd hidden layer	Output layer
t_{90}	9	10	–	–	1
Hardness	9	10	–	–	1
Density	9	10	–	–	1
Abrasion loss	9	3	–	–	1
Crosslink density	9	10	–	–	1
Elongation at break	9	10	–	–	1
Tensile stress at break	9	10	–	–	1
Displacement at tear	9	10	5	–	1
Tear Force	9	10	8	5	1

ANN was created and structured, the training process was carried out using the dataset obtained from laboratory experiments. In this way, the input weights of each neuron were adjusted to model the dataset, enabling the prediction of the properties of the composite under study.

Fig. 1 shows the schematic architecture of the ANN developed to predict the maximum force in the tear resistance test. Among the nine models created, this ANN has the most complex structure, featuring three hidden layers with 10, 8, and 5 neurons, respectively.

To carry out the training process of the ANNs using the dataset obtained from the mechanical property tests of the BR and rCB composites, this study employed the Levenberg-Marquardt training algorithm with Bayesian regularization. It is worth noting that the training function with Bayesian regularization is characterized by the application of Bayesian inference mechanisms in the adjustment of ANN weights, by computing a probability density function over all possible parameters of the network [43].

Bayesian ANNs are probabilistic graphical models that, using a directed acyclic graph, establish the dependency relationships between variables in the dataset. They are therefore suitable for modeling uncertainty and performing probabilistic inference, achieving superior performance with smaller datasets or, in the case of experimental data, when spurious results are present [35]. Moreover, they combine the modeling potential of ANNs with the analytical robustness of Bayesian statistics, thus avoiding typical issues of conventional neural networks, such as lack of convergence with small datasets (leading to high computational costs) and the risk of overfitting, which results in poor generalization.

Using MATLAB R2024b, along with its add-ons Deep Learning Toolbox (v.23.2) and Statistics and Machine Learning Toolbox (v.23.2), ANNs were developed and trained to predict each mechanical property of the rubber composites based on the rCB content. MATLAB 2024b was selected for this purpose due to its graphical interface and integrated tools for error plotting, regression analysis, performance evaluation, cross-validation, and gradient visualization. Additionally, it supports the Levenberg-Marquardt training algorithm with Bayesian regularization, which is particularly suitable for datasets of the size generated by the rheological and mechanical tests conducted in this study.

The dataset of mechanical properties for the BR/rCB composites consists of 72 samples, each comprising ten distinct properties, listed as follows:

- rCB content (phr);
- Optimum cure time (t_{90}) in minutes;
- Hardness (Shore A);
- Density (g/cm^3);
- Abrasion loss (mm^3/40 m);
- Crosslink density (mol/cm^3);
- Elongation at break (%; tensile strength test);
- Tensile strength at break (MPa; tensile strength test);
- Displacement at tear (mm; tear strength test);
- Tear force (N; tear strength test).

Although the dataset of 72 samples proved adequate for modeling, an increase in the total number of samples, either by including additional formulations or by increasing the number of replicates per formulation, could theoretically enhance the models' generalization capacity and robustness. To mitigate the risk of overfitting and ensure generalization, the Levenberg-Marquardt algorithm with Bayesian regularization (trainbr() in MATLAB) was used during network training. This algorithm modifies the original cost function by incorporating a penalty term on the synaptic weights, which controls model complexity and promotes improved generalization even when working with relatively small datasets.

In the context of this study, the training process begins with the creation of the ANN architecture, during which the input features (known properties), the target property to be predicted, the training algorithm, the number of hidden layers, and the number of neurons in each hidden layer are defined. Once the ANN structure is established, training proceeds with analysis of the experimental dataset: the network calculates the predicted value of the target property based on the remaining inputs, compares it with the experimentally determined value, and records the error.

This process is repeated for each sample in the dataset, completing one training cycle known as an epoch. At the end of each epoch, the training procedure computes the Mean Squared Error (*MSE*) and the Mean Absolute Relative Error (*MARE*) as statistical indicators of the convergence of the trained ANN model. The training process advances through successive epochs, and if the mean squared error (*MSE*) remains high, indicating a lack of convergence, additional epochs are executed. The maximum number of training epochs is defined at the start of the process, with the default value in the MATLAB Deep Learning Toolbox set to 1000 epochs. However, as noted, the software monitors error values during training and automatically stops when the minimum error is reached, [37], indicating convergence of the ANN, as illustrated in Fig. 2.

The most commonly used metrics for evaluating the performance of

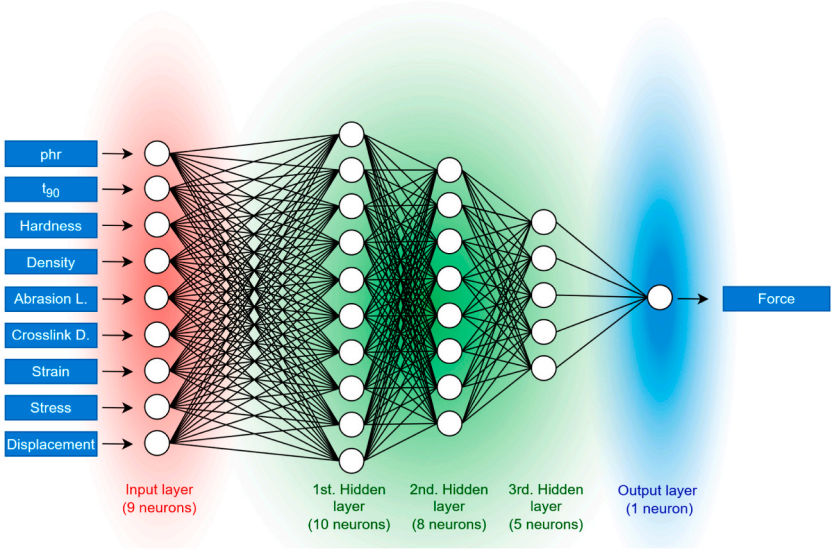

Fig. 1. Architecture of the ANN for predicting the tear force in the tear resistance test.

Fig. 2. Training parameters (a) and performance (b) of an ANN in MATLAB 2024b.

neural network training are the mean squared error (*MSE*), the mean absolute relative error (*MARE*), and the coefficient of determination (R^2). These metrics are calculated based on the difference between the predicted and the actual values [44], as expressed in Equations (5)–(7):

$$MSE = \frac{1}{n} \cdot \sum_{i=1}^{n} (y_i - \hat{y}_i)^2 \tag{5}$$

$$MARE = \frac{1}{n} \cdot \sum_{i=1}^{n} \left| \frac{y_i - \hat{y}_i}{y_i} \right| \tag{6}$$

$$R^2 = 1 - \frac{\sum (y_i - \hat{y}_i)^2}{(y_i - \bar{y})^2} \tag{7}$$

Where:
MSE = mean squared error
$MARE$ = mean absolute relative error
R^2 = coefficient of determination
n = number of samples
y_i = actual value
$\hat{y}_i$ = predicted value
$\bar{y}$ = mean of actual values

The *MSE* measures the average error between the fitted and actual values by squaring the difference; the lower the value, the better the ANN performance. The *MARE* quantifies the mean absolute relative error with respect to the expected value and is expressed as a percentage. As with *MSE*, since it represents error magnitude, lower *MARE* values (ideally close to zero) indicate better model performance. The R^2, in turn, measures how much of the data variability is represented by the model, ranging from –∞ to 1, with 1 being ideal, indicating perfect and faithful adjustment of the model to the training data.

The importance of these statistical metrics is supported by numerous scientific studies that adopt them to evaluate the results obtained through the application of different artificial intelligence (AI) techniques. For instance, Padmavathi (2005) [45], employed R^2 and *MSE* to evaluate the performance of ANNs designed to predict Mooney viscosity and fluid viscosity from process variables in BR manufacturing. Abdollahzadeh (2011) [46], developed ANNs to predict soil erosion in the Jajuko Rachidani basin, in Tanakami, Japan, using *MARE*, *MSE*, and R^2 to assess model performance and compare ANN predictions with those from multiple linear regression (MLR). Almaliki (2016) [47], used *MSE* and R^2 to evaluate the performance of Levenberg-Marquardt ANNs for predicting agricultural tractor performance in drawbar power, fuel consumption, rolling resistance, and traction efficiency. Rezazadeh and Naderpour (2019) [48], applied R^2 and *MSE* to monitor ANN performance for predicting shear strength and vertical deformation of rubberized concrete composites. In the same year, Onoji (2019) [49], used *MARE* and absolute average deviation (*AAD*) to compare the performance of response surface methodology (RSM) and ANN for predicting oil yield from underutilized rubber seed, obtaining superior results with ANN. Abdelkareem (2022) [50] also used *MSE* and R^2 as performance criteria in the training of ANNs designed to evaluate hydrogen production technologies, aiming to maximize hydrogen output while minimizing production costs.

The neural networks were developed using programming code and subjected to a training process. Throughout training, model performance is continuously monitored by the software, which provides statistical indicators of error, such as the error histogram illustrated in Fig. 3. The training was conducted using the Levenberg-Marquardt algorithm with Bayesian regularization, which is particularly well-suited for relatively small datasets and helps prevent overfitting.

Once an acceptable level of learning was achieved, as indicated by the *MSE* and *MARE* metrics, the ANN was stored and could then be used to predict a specific property of the evaluated composite. It is important to emphasize that this process was conducted independently for each of the nine properties assessed in this study, resulting in a set of nine independently trained ANNs, each computationally modeling one property of the studied composite.

Each ANN, trained to predict a given property, requires as input a set of *n-1* values, where *n* is the total number of properties in the dataset. From this set, the ANN uses the value of rCB content in phr and the estimated values of the other eight properties to predict the property for which it was trained. Thus, it can estimate the value of the target property and calculate the prediction error based on the experimentally obtained laboratory value.

Once the ANNs were trained and validated, they were implemented in an application developed in this study to predict the nine properties of rubber composites with rCB, based on a given rCB content input by the user. It should be noted that the experimental tests were conducted for six formulations with rCB contents ranging from 0 to 50 phr in

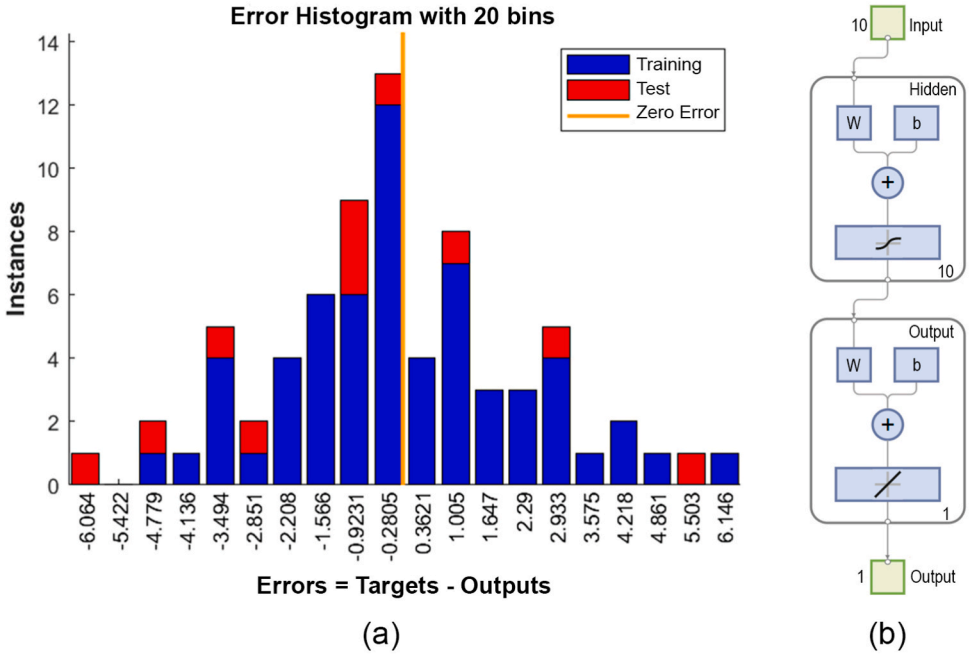

Fig. 3. Error histogram of the artificial neural network for t_{90} prediction (a) and structure of the artificial neural network with an input layer with ten neurons, one hidden layer containing ten neurons and an output layer with one neuron (b).

increments of 10 phr. Since each ANN requires values of the other properties to predict the property it was trained to model, the developed application supplies the ANNs with weighted average values based on the provided rCB content and the experimental dataset, thereby enabling an initial estimation.

To calculate the weighted means, the algorithm uses the phr values immediately below and above the user-specified phr. For each phr level evaluated experimentally, twelve specimens were tested. Due to the inherent variability of experimental data and the occasional presence of outliers, the algorithm incorporates a mechanism to discard the highest and lowest results for each phr level. This is done using MATLAB's internal mean function trimean(), which improves the robustness of the input data.

Thus, each initial estimation is calculated automatically using Equation (8), which determines the weighted average between the internal means of the experimental values for the nearest phr levels (multiples of 10 phr) immediately below and above the phr of interest:

$$E = M_{\text{inf}} + \left(\left(M_{\text{sup}} - M_{\text{inf}} \right) \cdot \left(\frac{phr_{pred} - phr_{\text{inf}}}{phr_{\text{sup}} - phr_{\text{inf}}} \right) \right) \quad (8)$$

Where:

E = estimated value of a mechanical property

M_{inf} = internal mean of the property for the phr value immediately below in the dataset

M_{sup} = internal mean of the property for the phr value immediately above in the dataset

phr_{pred} = phr value for which the prediction is being performed

phr_{inf} = phr value immediately below phr_{pred} in the dataset

phr_{sup} = phr value immediately above phr_{pred} in the dataset

In this way, it was possible to integrate the trained ANNs into a computational application in which, upon providing the desired rCB content (in phr), the program calculates and displays the predicted values of each property, as determined by the specific ANN associated with that property.

3. Results and discussion

3.1. Rheometry

Fig. 4 presents the rheometric curves of the BR composites with rCB. As shown in Table 3, the scorch time t_{S1} and the optimum vulcanization time t_{90} of the composites decrease with increasing filler content, while the minimum torque M_L gradually increases. This behavior is related to the increase in compound viscosity due to the addition of filler. The values of M_L indicate the viscosity of the unvulcanized compound, also reflecting its processability. The maximum torque M_H increases with the higher rCB content, revealing good interaction between the filler and the matrix as well as the formation of crosslinks. The torque variation ΔM quantifies the reinforcement of the elastomer's mechanical properties [51] and is commonly used as an indirect indicator of crosslink density [52].

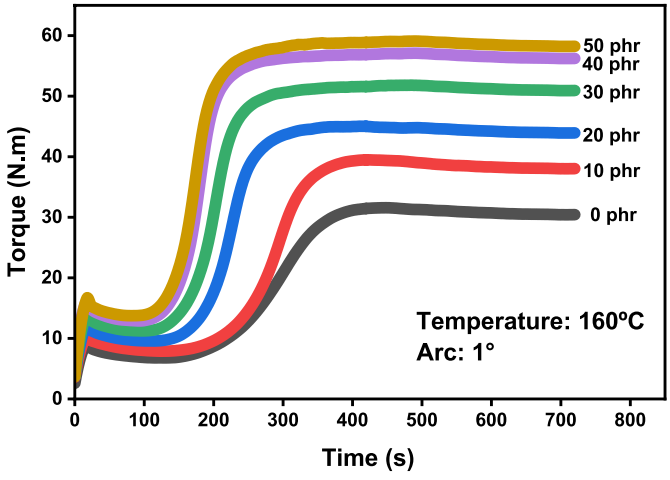

Fig. 4. Rheometric curves of BR-rCB composites from 0 to 50 phr.

Table 3
Rheometric test: means and standard deviations of minimum torque (M_L), maximum torque (M_H), torque variation (ΔM), scorch time (t_{S1}) and optimum cure time (t_{90}) of BR-rCB composites.

Formulation	M_L			M_H			ΔM			t_{S1}			t_{90}		
(phr)	(dN•m)			(dN•m)			(dN•m)			(min)			(min)		
0	0.665	±	0.005	3.129	±	0.031	2.464	±	0.030	1.927	±	0.126	6.166	±	0.058
10	0.815	±	0.014	3.965	±	0.419	3.150	±	0.034	1.918	±	0.169	5.373	±	0.120
20	0.941	±	0.009	4.533	±	0.377	3.592	±	0.037	1.652	±	0.130	4.554	±	0.026
30	1.13	±	0.010	5.180	±	0.536	4.050	±	0.048	1.424	±	0.132	3.906	±	0.076
40	1.278	±	0.008	5.633	±	0.305	4.355	±	0.029	1.353	±	0.103	3.580	±	0.030
50	1.363	±	0.012	5.870	±	0.582	4.507	±	0.054	1.244	±	0.101	3.614	±	0.063

3.1.1. Degree of rCB dispersion in the polymer matrix

The degree of dispersion (L) in the polymer matrix is a relative index based on the unfilled rubber and represents, inversely, the extent of filler dispersion within the matrix. Lower values of L indicate better filler dispersion. As shown in Fig. 5, the value of L increases with the addition of rCB. However, although L increases, the values remain very close to zero, indicating good dispersion of the filler within the matrix, which in turn facilitates the processability of the compound [53].

3.2. Relative density

The results obtained from the density tests of the composites, presented in Fig. 6, indicate that the density of the elastomer increases with the addition of higher amounts of rCB. This result was expected, as increasing the filler content in the same volume of elastomer proportionally increases the mass, thereby raising the final density of the composite.

3.3. Crosslink density

As shown in Fig. 7, the crosslink density increases with the rising rCB content in the composites. This behavior is attributed to the probable interaction between rCB and the rubber matrix, which can act as a pseudo-crosslink, hindering solvent penetration and thus being accounted for as a crosslinking point by the swelling method using the Flory-Rehner equation. This favorable filler-matrix interaction results from the good dispersion of the rCB particles [54,55]. Cruz (2024) [56], also observed an increase in the crosslink density of NR composites with rCB, despite no variation in the sulfur content or vulcanization system. Similarly, Ribeiro (2023) [57] reported that the strong interaction between the polymer matrix and the filler creates physical interaction sites that are interpreted as crosslinking points when evaluated by the swelling method with application of the Flory-Rehner equation. Most mechanical properties and microstructural characteristics of vulcanized rubber composites are highly dependent on the material's crosslink density [58].

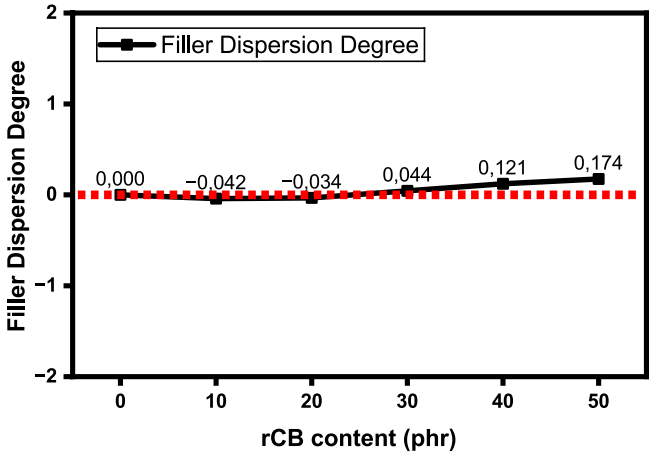

Fig. 5. Degree of filler dispersion in the polymer matrix.

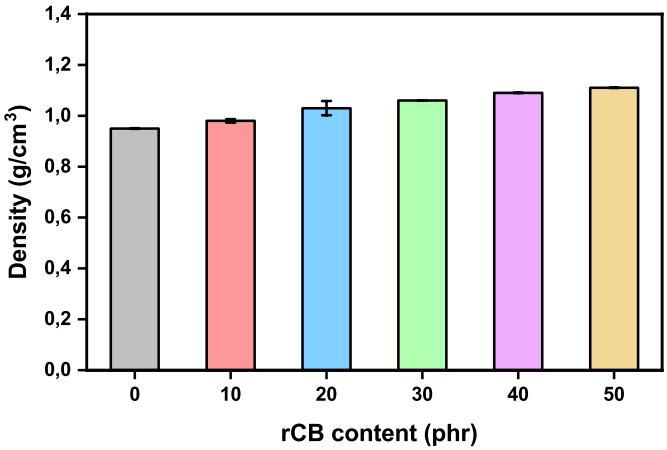

Fig. 6. Density of BR-rCB composites from 0 to 50 phr.

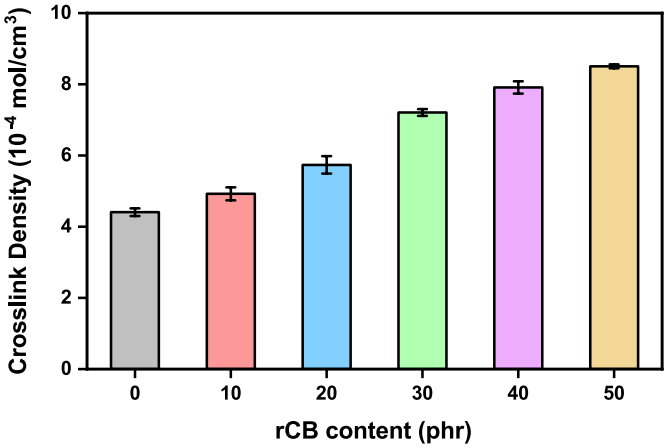

Fig. 7. Crosslink density as a funcion of rCB content.

3.4. Hardness

The hardness tests reflect the effects produced by variations in the crosslink density. At the microscopic level, an increased filler content restricts the mobility of polymer chains. As the amount of recovered carbon black (rCB) increases, the crosslink density also rises, which in turn results in greater hardness of the elastomer at the macroscopic scale, as illustrated in Fig. 8. This behavior is attributed to the structure formed after vulcanization with filler addition, where the interaction between the polymer chains and rCB promotes a structure more resistant to indentation by the durometer (Shore A).

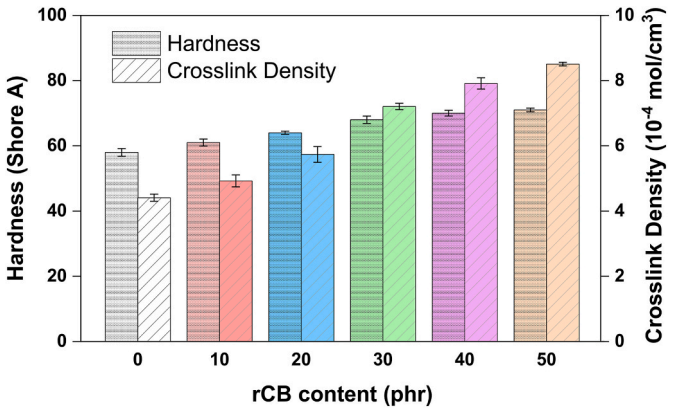

Fig. 8. Hardness and crosslink density from 0 to 50 phr.

3.5. Abrasion resistance

The abrasion loss test demonstrated that good filler dispersion, matrix homogeneity, low agglomerate formation, and increased crosslink density significantly improve the abrasion resistance of the rubber, as shown in Fig. 9. As the rCB content increases, a notable reduction in abrasion loss is observed, which can be clearly associated with the increase in crosslink density. Recovered carbon black tends to enhance adhesion to the polymer matrix.

3.6. Tensile and tear strength

As illustrated in Fig. 10, rCB provides mechanical reinforcement to the polymer matrix, enhancing both tensile and tear strength by requiring greater force to induce failure. This behavior is consistent with the findings of Wetchakama (2018) [49], where increasing filler content continuously improved the mechanical properties of BR filled with carbon black (CB). Such enhancement is attributed to the increased density of crosslinking and stronger interfacial adhesion forces between the filler surface and the elastomeric chains. As the rCB concentration increases, a structural network forms through interactions between the filler and the polymer chains, which connects with the chemically crosslinked network established by sulfur bridges between the polymer chains. This interconnection leads to the formation of a superstructure responsible for the observed mechanical reinforcement [59]. Moreover, the effective dispersion of rCB particles reduces the occurrence of agglomerates and promotes interfacial interaction between the filler and the rubber matrix.

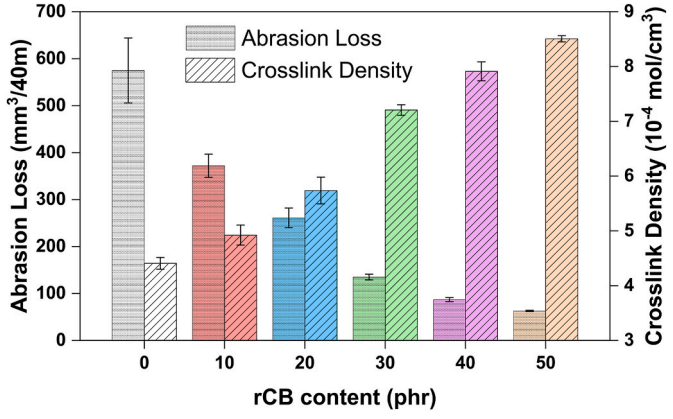

Fig. 9. Abrasion loss and crosslink density for BR-rCB formulations from 0 to 50 phr.

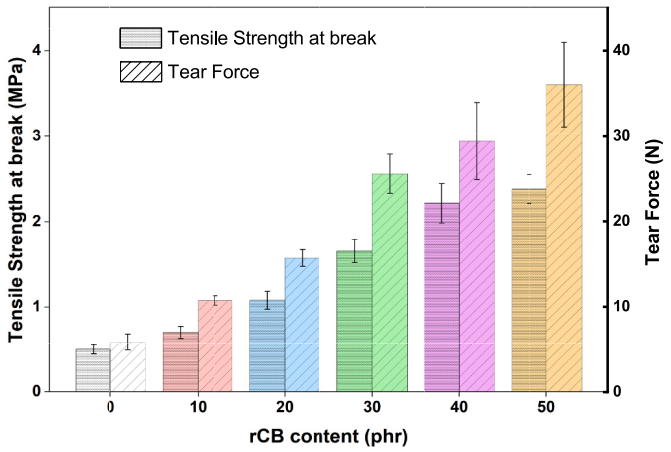

Fig. 10. Tensile strength and tear force in tensile and tear resistance tests.

3.7. Artificial neural networks

Following the completion of rheometric and mechanical property tests, seventy-two samples of BR composites with rCB were obtained, with filler contents ranging from 0 to 50 phr in increments of 10 phr for each set of twelve samples. Ten distinct properties were measured for each sample.

Using the data generated from the laboratory experiments, an ANN was trained for each property of the composite under study, as described in the experimental procedures. After training the ANNs, the error values were calculated and are presented alongside the architecture of each ANN in Table 4.

During the training phase of the ANNs, the models demonstrated excellent statistical performance, reflected by consistently low *MARE* and *MSE* values, along with high R^2 values for nearly all evaluated properties. For example, the lowest *MARE* (0.00015) and a null *MSE* (0.000000), associated with an R^2 of 1.000, were observed for abrasion loss, indicating an almost perfect fit between the experimental data and the model predictions during training.

Overall, the models achieved R^2 values above 0.96 for all properties, demonstrating a strong ability to represent the input data. Density remained among the highlights in terms of accuracy, with a *MARE* of only 0.004977 and an *MSE* of 0.000130, reinforcing its stable predictability even in the presence of variability associated with rCB. Although its R^2 value (0.962889) was slightly lower than those observed for other properties, the associated error metrics indicate the model's excellent performance for this variable. Since R^2 can be sensitive to the data variability and the presence of potential outliers, the combined use of additional error metrics is essential for a more robust assessment. Therefore, considering the low *MARE* and *MSE*, it can be concluded that the model exhibits good generalization capacity for this property, even

Table 4
ANN architecture and performance tests (error statistics).

ANN	Architecture[a]	*MARE*	*MSE*	R^2
t_{90}	9/10/1	0.009294	12.762164	0.996241
Hardness	9/10/1	0.010364	0.733291	0.974413
Density	9/10/1	0.004977	0.000130	0.962889
Abrasion loss	9/3/1	0.000150	0.000000	1.000000
Crosslink density	9/10/1	0.019586	0.048090	0.979746
Elongation at break	9/10/1	0.034940	5.844994	0.979416
Tensile strength at break	9/10/1	0.035285	0.006013	0.988851
Displacement at tear	9/10; 5/1	0.021217	0.294487	0.988058
Tear force	9/10; 8; 5/1	0.091706	2.000007	0.985416

[a] Architecture: number of neurons in the input layer/number of neurons in the 1st hidden layer; number of neurons in the 2nd hidden layer; number of neurons in the 3rd hidden layer/number of neurons in the output layer.

when trained on a relatively small dataset.

The highest *MARE* during training was observed for the maximum tear force (0.091706), which may be related to the greater complexity of the network architecture (9/10; 8; 5/1) and to the potential sensitivity of this property to microstructural variations in the composite. Nevertheless, the model achieved an R^2 of 0.985416, suggesting that, despite the higher relative error, the overall fit remained excellent.

Similar to the trends observed in the experimental tests used for predictions confirmation, the lowest training errors were also concentrated in the models for density, abrasion loss, and tear displacement, indicating that these variables exhibit more stable and predictable behavior in response to the input features. This consistency between training and validation results reinforces the robustness of the developed models and suggests that the artificial neural networks effectively captured the relationships between composite formulation and the corresponding mechanical and rheological properties.

It is worth noting that the Levenberg-Marquardt algorithm with Bayesian regularization (trainbr() function in MATLAB) was used for network training. This algorithm automatically adjusts regularization parameters to control network complexity, contributing significantly to training stability and generalization capacity, even in cases where R^2 values may appear slightly lower. This approach is particularly effective when working with relatively small datasets, as in the present study, and reinforces the reliability of the results obtained.

Řeháčková (2023) [20] also employed R^2 and *MARE* as reliability indicators in data modeling using ANNs in her research. To monitor ANN performance after the training phase, performance plots using the *MSE* metric and error histograms can be used to assess the proximity between predictions and experimental values. The error histograms and performance plots for the ANNs trained in this study are presented in Figs. 11 and 12, respectively.

With the trained ANNs developed to model the laboratory experiments, an additional application test was proposed. For this purpose, a value of 23 phr was randomly selected, which had not been used in the initial procedures that served as the basis for the training of the ANNs. This value was provided to the application developed to obtain the predicted values of the mechanical properties modeled by the ANNs. As mentioned in the experimental procedures, since each ANN is trained to predict a single property, it requires input values for the remaining properties. Therefore, for each mechanical property used as input to the ANN, an initial estimate was calculated using the weighted average method, as presented in Equation (8). To illustrate this procedure, Table 5 presents the input values used in the prediction of t_{90} for BR composites containing 23 phr of rCB. Fig. 13 shows the command

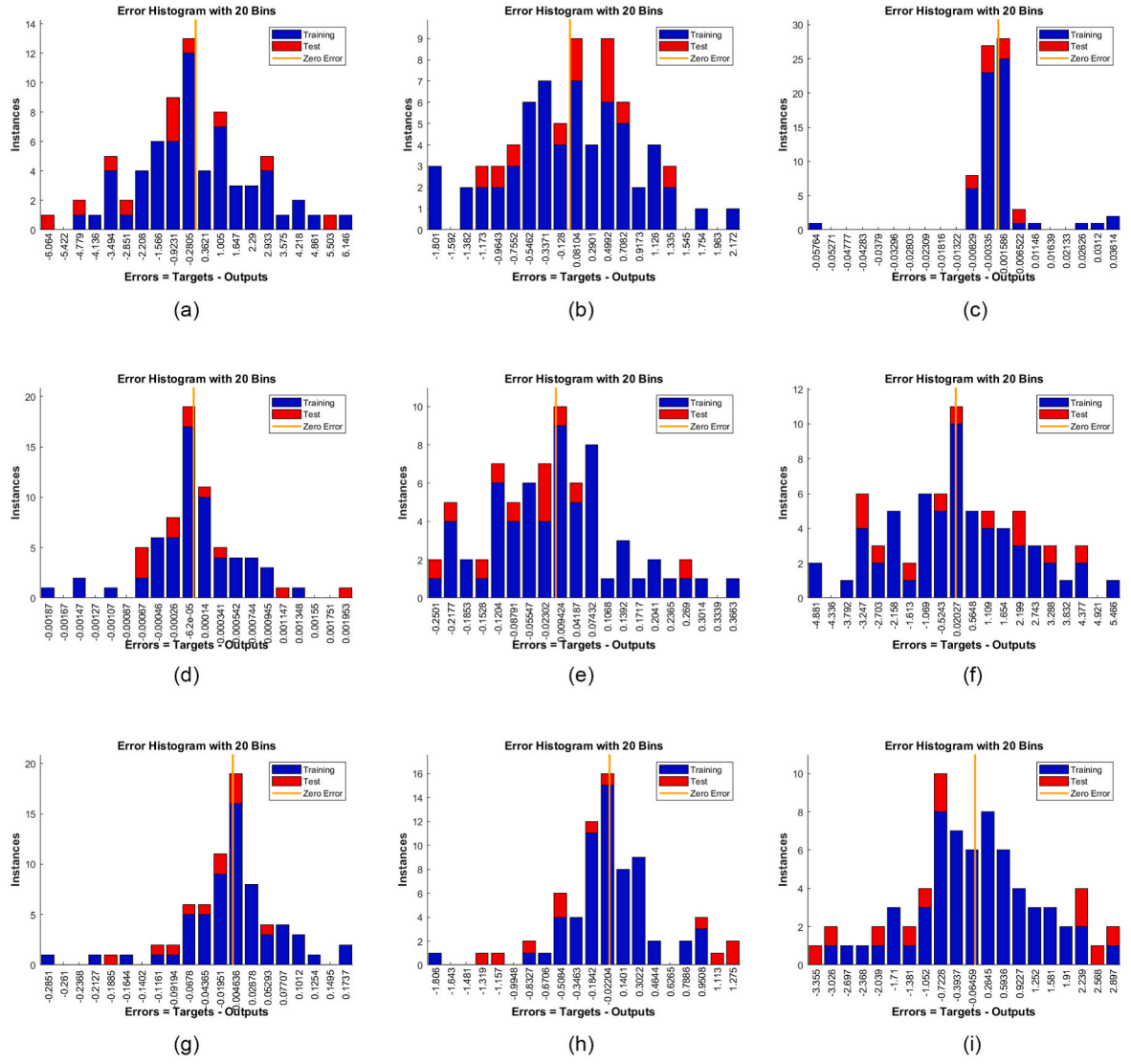

Fig. 11. Error histograms of the ANNs training process:(a) t_{90}; (b) hardness; (c) density; (d) abrasion loss; (e) crosslink density; (f) elongation at break; (g) Tensile strength at break; (h) displacement at tear; (i) tear force.

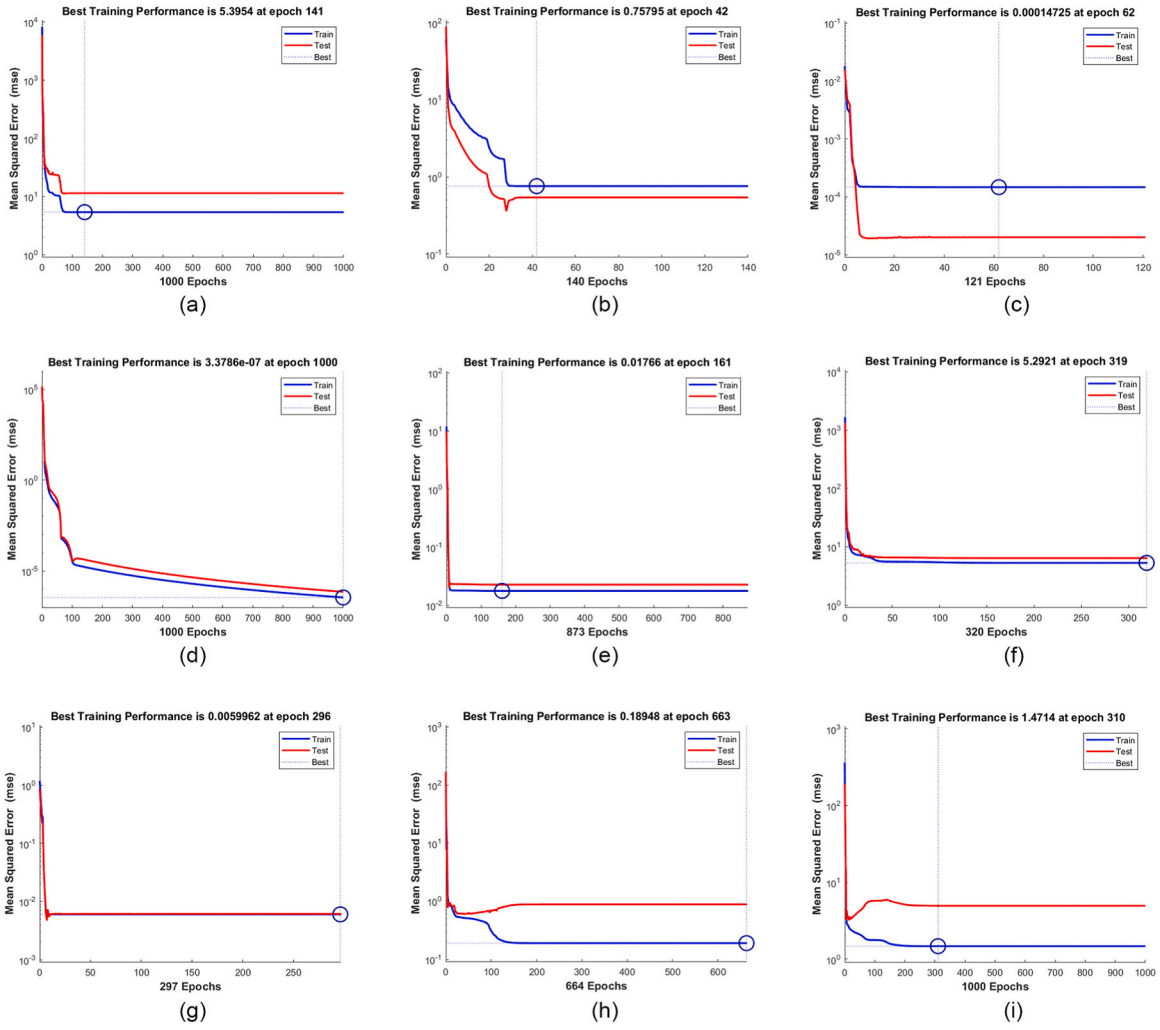

Fig. 12. Performance metrics of the trained ANNs: (a) t_{90}; (b) hardness; (c) density; (d) abrasion loss; (e) crosslink density; (f) elongation at break; (g) Tensile strength at break; (h) displacement at tear; (i) tear force.

Table 5
Input and output values of the ANN for the prediction of t_{90}.

Property	Input value	Description of the input value	ANN output value
rCB content (phr)	23	Arbitrary	
Optimum cure time t_{90} (s)	Not provided	To be predicted by the ANN	256.9302
Hardness (Shore A)	65.732	Calculated according to Equation 8	
Density (g/cm^3)	1.0447	Calculated according to Equation 8	
Abrasion loss (mm^3/40 m)	223.1649	Calculated according to Equation 8	
Crosslink density (10^{-4} mol/cm^3)	6.1717	Calculated according to Equation 8	
Elongation at break (%)	57.3177	Calculated according to Equation 8	
Tensile strength at break (MPa)	1.2504	Calculated according to Equation 8	
Displacement at tear (mm)	18.3072	Calculated according to Equation 8	
Tear force (N)	18.6075	Calculated according to Equation 8	

window displaying the execution of the ANN for the prediction of t_{90} of these composites.

For each mechanical property, it was necessary to develop a distinct neural network, requiring the nine ANNs to be executed sequentially for the prediction of each mechanical property of BR-rCB with the same filler content. As an improvement to the user interface, aiming to streamline software usability, the integration of the ANNs into a single application was implemented, so that only the amount of rCB (in phr) needs to be provided. Considering the desired rCB content, the application runs all nine ANNs and outputs a data matrix containing the predicted values for each of the nine mechanical properties studied, as illustrated in Fig. 14.

As previously mentioned, an additional test was performed using a formulation containing 23 phr of recovered carbon black (rCB), a value not included in the initial training dataset used for the ANNs. This input was provided to the developed application (Fig. 14), and the predicted mechanical properties are summarized in Table 6.

To validate the reliability of these predictions, laboratory tests were performed on the BR-rCB composite formulated with 23 phr in quintuplicate. The experimental results are summarized in Table 7.

A comparison between the predicted values and the experimental data for the 23 phr formulation reveals prediction errors ranging from −5.08 % to 8.09 %, as illustrated in Fig. 15, such discrepancies are justifiable given the nature of rCB, which, unlike virgin carbon black (CB), exhibits variability in its chemical composition due to the heterogeneous origin of recycled materials.

While the use of a single rCB source (PX-300) may be considered a limitation regarding the generalization potential of the developed

```
>>load('C:\...\4.PESQUISA\RNA\TrainedRNAs\02.RNA_PredT90-02_-6.0_6.1_10c')
net([23; 65.732; 1.04477835315838; 223.164961127296; 6.1717563330657; 57.31771; 1.25041;
18.30723; 18.60753])
ans = 256.9302
```

Fig. 13. Example of t_{90} prediction execution by the corresponding neural network.

```
Enter the PHR for which you want to calculate the rheometric and mechanical properties: 23

avgParameters =
23  261.57 65.732 1.0448 223.1656.1718 57.31771.2504 18.307218.6075

predictedParameters =
23  256.9302   65.85561.0411 223.1663   6.1955 58.31081.246  18.127 18.6638
```

Fig. 14. Example of execution of the developed application integrating the trained ANNs.

Table 6
ANN predictions for BR-rCB composites with 23 phr rCB.

Property	ANN predictions
rCB content (phr)	23
Optimal cure time t_{90} (s)	256.9302
Hardness (Shore A)	65.8556
Density (g/cm^3)	1.0411
Abrasion loss (mm^3/40 m)	223.1663
Crosslink density (10^{-4} mol/cm^3)	6.1955
Elongation at break (%)	58.3108
Tensile strength at break (MPa)	1.246
Displacement at tear (mm)	18.127
Tear force (N)	18.6638

Table 7
Experimental results for BR-rCB composites with 23 phr of rCB.

Property	Experimental results
rCB content (phr)	23
Optimal cure time t_{90} (s)	270.67
Hardness (Shore A)	63.17
Density (g/cm^3)	1.0207
Abrasion loss (mm^3/40 m)	228.20
Crosslink density (10^{-4} mol/cm^3)	5.732
Elongation at break (%)	60.09
Tensile strength at break (MPa)	1.19
Displacement at tear (mm)	18.21
Tear force (N)	18.44

models, the scope of this study is focused on applying artificial neural networks as a predictive tool for specific elastomer formulations containing a defined type of rCB, rather than developing a generalist model applicable to multiple sources of this recovered material.

A detailed analysis of the prediction errors provides further insight into the sensitivity of the models to different composite properties. The highest absolute error was observed in the prediction of crosslink density, with a deviation of approximately 8.09 %. This property is strongly influenced by molecular-level structural factors such as the degree of unsaturation in the base rubber, the presence of polar residues in the rCB, and the efficiency of vulcanization. These variables are prone to fluctuations that may be difficult to capture using only the available input data. Moreover, the determination of crosslink density through swelling tests involves indirect measurements and theoretical assumptions such as the Flory-Rehner theory, which may introduce additional uncertainty into the dataset.

In contrast, the smallest absolute error was observed for tear

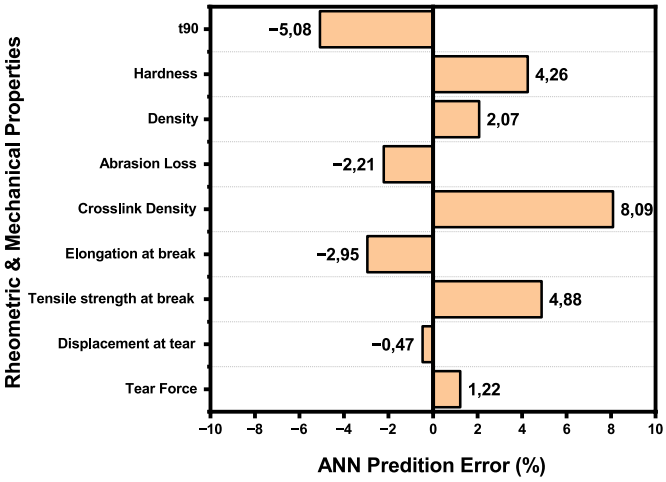

Fig. 15. Relative prediction errors compared to laboratory test results.

displacement, with a deviation of only 0.47 %, possibly due to its stronger correlation with mechanical properties more directly affected by the polymer matrix and the distribution of rCB. This property may exhibit lower experimental variability and greater stability against minor formulation fluctuations, which facilitates learning by the model.

Overall, properties that are directly related to the composite's three-dimensional microstructure, such as crosslink density and tensile strength, tend to be more complex to model. On the other hand, more macroscopic and integrative properties, such as displacement and density, demonstrate higher predictability. These results underscore the importance of understanding the underlying physical and chemical nature of each property when applying machine learning-based modeling approaches.

Considering that rCB originates from a diverse range of vulcanized rubber formulations tailored for various applications and manufacturers, the deviations between predicted and experimental values fall within acceptable limits. Dwivedi (2020) [60], reported that the incorporation of rCB reduced t_{90}, enhanced tensile strength and elongation at break, but decreased tensile modulus and tear resistance compared to unfilled rubber. The author attributed these effects to reduced interactions between filler particles and polymer chains caused by carbonaceous residues blocking active surface sites. Similarly, Norris (2023) [61], emphasized that while residual carbon on rCB surfaces is widely recognized, its exact contribution to mechanical reinforcement

remains difficult to isolate due to the heterogeneous nature of scrap tire feedstocks.

Fig. 16 shows the correlation between the ANN predictions and the experimental measurements, demonstrating a strong agreement between the modeled and observed values.

Overall, the highest prediction error observed was approximately 8 %, recorded for crosslink density, while the lowest error was below 1 %, observed for tear displacement. These variations reflect the specificity of each ANN model, which was independently trained and structured to predict different composite properties.

The results highlight the advantages of using artificial neural networks compared with estimates obtained by weighted averages of internal means. Interpolation is limited to discrete values derived directly from formulations containing 0, 10, 20, 30, 40, and 50 phr of rCB, and it is applied independently to each property without ensuring multivariate coherence across the results. In contrast, ANNs trained with the same set of experimental formulations were employed to generate predictions at intermediate concentrations (3, 5, 7, 13, 15, 17 phr, among others), enabling a continuous analysis of property behavior across the entire composition range.

This aspect is particularly relevant because the predictive model is not restricted to isolated points but is able to estimate trends consistently between the experimental extremes, as illustrated in Fig. 17. The comparison at 23 phr of rCB shows that, although both approaches exhibit relatively small deviations from laboratory tests, ANNs provide closer agreement in critical properties such as the optimum vulcanization time (t_{90}) and elongation at break, which are highly sensitive to processing conditions and final composite performance. Therefore, while interpolation is useful only as an initial approximation, ANNs deliver a more robust and reliable predictive model that can be continuously refined with the incorporation of new data and applied to the development of formulations not experimentally tested.

In Fig. 17, it can be observed that interpolation applied to the points predicted by the ANNs results in smoother curves that are consistent with the expected behavior of elastomeric composites, whereas direct interpolation using internal means produces only linear segments between points.

When linear regression is applied to the estimates obtained by weighted averages of internal means, the discrepancy becomes even more pronounced. The use of ANNs is justified by the physicochemical complexity of the analyzed composites, where nonlinear interactions among the polymer matrix, rCB, and other additives significantly influence mechanical and rheometric properties. Linear or tree-based models, while relevant in other contexts, offer no clear advantage in predictive capacity for the current dataset and may require computational effort and parameter tuning comparable to that of ANNs without guaranteeing additional improvements.

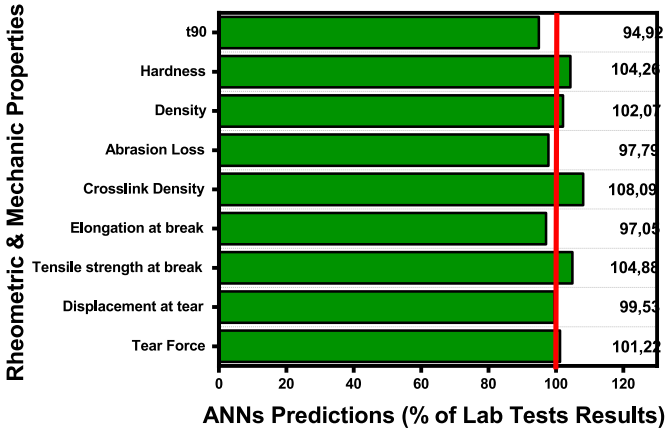

Fig. 16. Correlation between ANN predictions and laboratory test results.

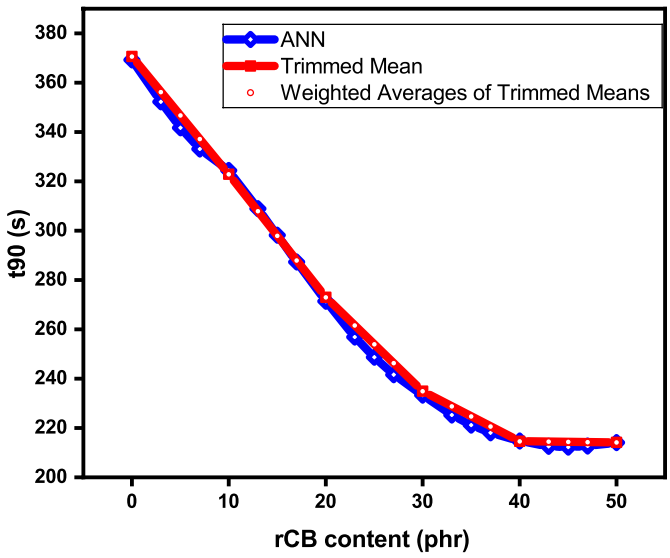

Fig. 17. Comparison of ANN predictions with estimates obtained by weighted averages of internally trimmed means.

Figs. 18 and 19 presents a comparison between the predictions from the proposed system and the results obtained by linear regression, clearly showing that ANNs provide a more consistent fit to the experimental data and better capture the underlying trends.

Although this study focused exclusively on the application of artificial neural networks for predicting the mechanical properties of elastomeric composites containing PX-300 rCB as the sole reinforcing filler, it is acknowledged that including formulations with virgin CB or other types of rCB would allow for direct comparison between materials derived from different filler sources. Such comparisons would add value to the analysis by more clearly elucidating the specific impact of compositional variability in rCB on composite performance.

However, the proposed approach was intentionally constrained to assess the predictive potential of neural networks in a technically challenging scenario, characterized by the heterogeneity of rCB

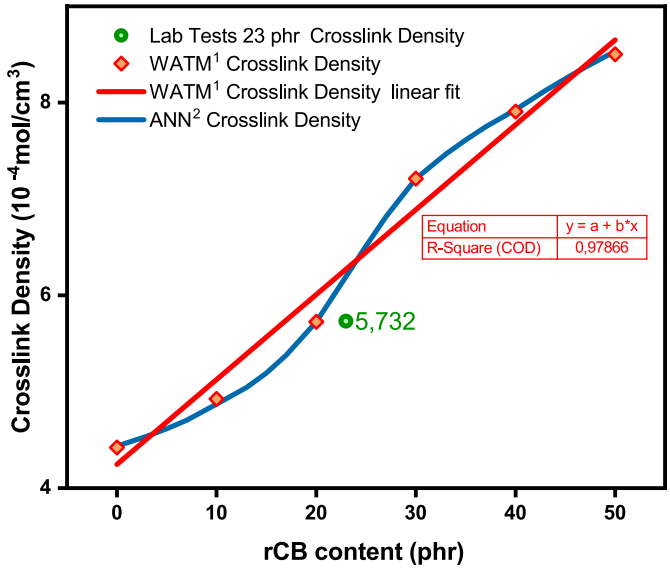

[1] WATM: Weighted Averages of Trimmed Means
[2] ANN: Artificial Neural Network

Fig. 18. Comparison between ANN predictions and estimates obtained by weighted averages of internally trimmed means for crosslink density.

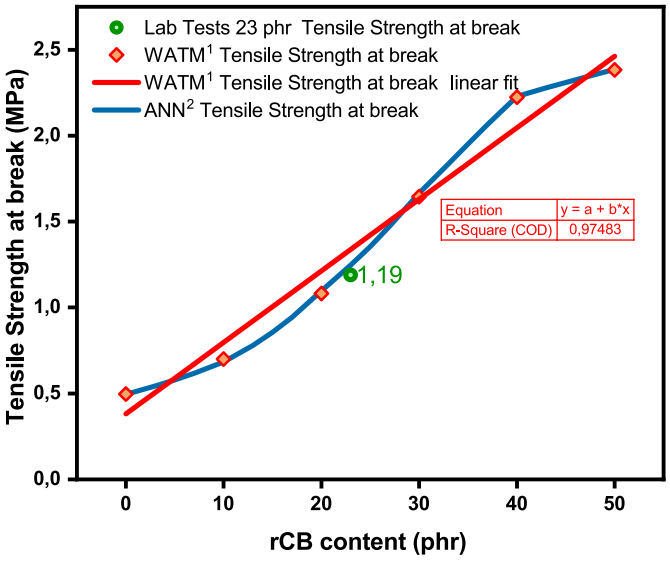

[1] WATM: Weighted Averages of Trimmed Means
[2] ANN: Artificial Neural Network

Fig. 19. Comparison between ANN predictions and the linear fit of weighted averages of internally trimmed means for tensile strength at break.

obtained from the pyrolysis of end-of-life tires. Even so, the developed models showed consistent performance. For instance, the density property exhibited low *MARE* (0.004977) and *MSE* (0.000130) values, despite a slightly lower R^2 (0.962889). These results suggest that the neural network could capture relevant patterns in the data, even in the presence of the high variability associated with the filler used.

In this context, future studies could incorporate formulations containing virgin CB as a reference to enable more comprehensive comparative analyses and to further deepen the understanding of the behavior of conventional fillers versus sustainable alternatives such as rCB.

4. Conclusion

The rCB, despite its secondary origin, demonstrated significant reinforcing performance in the analyzed polybutadiene-based elastomeric composites. Increasing rCB content resulted in higher hardness and crosslink density, suggesting effective surface interactions between the filler and the polymer chains. These interactions contributed to improvements in abrasion, tensile, and tear resistance, indicating the formation of a reinforced, cohesive structure and increased material stiffness.

The predictive modeling using ANNs proved effective in estimating the rheometric and mechanical properties of the rCB-filled composites, with prediction errors within acceptable limits. The ANN-based approach enabled the optimization of compound formulations based on target properties, reducing reliance on empirical trial-and-error methods, minimizing material waste, and lowering operational costs.

This study highlights both the potential of rCB as a sustainable functional filler and the applicability of artificial intelligence techniques in materials engineering. As a future perspective, expanding the dataset to include different rubber matrices, filler types, curing systems, and additives is recommended to enhance the generalizability and predictive accuracy of the developed models in more complex elastomeric systems.

Declaration of competing interest

The authors declare that they have no known competing financial interests or personal relationships that could have appeared to influence the work reported in this paper.

Acknowledgements

To the São Paulo Research Foundation (FAPESP) for the financial support provided under grant number 2024/04118-0 and CNPq/Brazil, Process: 306108/2024-0.

References

[1] Smithers. Tire industry rebounds to reach $264.0 billion in 2021, and $325.6 billion in 2026 according to latest smithers research. Available from: https://www.smithers.com/resources/2021/november/tire-industry-rebounds-to-$264-billion-in-2021.
[2] Araujo-Morera J, Castro-Fresno D, Rodríguez-Hernández J, Gómez-Gil J. Sustainable mobility: the route of tires through the circular economy model. Waste Manag 2021;126:309–22. https://doi.org/10.1016/j.wasman.2021.03.025.
[3] Alvarez J, Lopez G, Amutio M, Artetxe M, Bilbao J, Olazar M. Evaluation of the properties of tyre pyrolysis oils obtained in a conical spouted bed reactor. Energy 2017;128:463–74. https://doi.org/10.1016/j.energy.2017.03.163.
[4] Lopez G, Artetxe M, Amutio M, Bilbao J, Olazar M. Waste truck-tyre processing by flash pyrolysis in a conical spouted bed reactor. Energy Convers Manag 2017;142:523–32. https://doi.org/10.1016/j.enconman.2017.03.051.
[5] Antoniou N, Zabaniotou A. Re-designing a viable ELTs depolymerization in circular economy: pyrolysis prototype demonstration at TRL 7, with energy optimization and carbonaceous materials production. J Clean Prod 2018;174:74–86. https://doi.org/10.1016/j.jclepro.2017.10.319.
[6] European Tyre & Rubber Manufacturers' Association (ETRMA). End-of-life tyres in a circular economy: ETRMA's perspective on a competitive recycling sector. Brussels: ETRMA; 2025. Available from: https://www.etrma.org/news/end-of-life-tyres-in-a-circular-economy-etrmas-perspective-on-a-competitive-recycling-sector/.
[7] World Business Council for Sustainable Development (WBCSD). Perspectives on end-of-life tire (ELT) management. Geneva: WBCSD; 2023. Available from, https://tireindustryproject.org/wp-content/uploads/2023/08/WBCSD_TIP_Perpectives-End-of-Life-Tire-Management_ELT_tires_sustainability.pdf.
[8] Landi D, Vitali S, Germani M. Environmental analysis of different end of life scenarios of tires textile fibers. Proced CIRP 2016;48:508–13. https://doi.org/10.1016/j.procir.2016.03.141.
[9] Martínez JD, Puy N, Murillo R, García T, Navarro MV, Mastral AM. Waste tyre pyrolysis – a review. Renew Sustain Energy Rev 2013;23:179–213. https://doi.org/10.1016/j.rser.2013.02.038.
[10] Song Z, Yang Y, Zhou L, Liu L, Zhao X. Gaseous products evolution during microwave pyrolysis of tire powders. Int J Hydrogen Energy 2017;42(29):18209–15. https://doi.org/10.1016/j.ijhydene.2017.04.169.
[11] Zhang Y, Wu C, Nahil MA, Williams P. High-value resource recovery products from waste tyres. Proc Inst Civ Eng Waste Resour Manag 2016;169(3):137–45. https://doi.org/10.1680/jwarm.16.00001.
[12] Hossain MS, Islam MR, Rahman MS, Kader MA, Haniubet H. Biofuel from co-pyrolysis of solid tire waste and rice husk. Energy Proc 2017;110:453–8. https://doi.org/10.1016/j.egypro.2017.03.168.
[13] Valente M, Sambucci M, Chougan M, Ghaffar SH. Composite alkali-activated materials with waste tire rubber designed for additive manufacturing: an eco-sustainable and energy saving approach. J Mater Res Technol 2023;24:3098–117. https://doi.org/10.1016/j.jmrt.2023.03.213.
[14] Antoniou N, Zabaniotou A. Experimental proof of concept for a sustainable end of life tyres pyrolysis with energy and porous materials production. J Clean Prod 2015;101:323–36. https://doi.org/10.1016/j.jclepro.2015.03.101.
[15] Abd El-sadek MS, Hassan MA, Nassar AM, El-Nashar DE, Fathy HM. Ethylene vinyl acetate as a multifunctional compatibilizer for improving the dispersion and mechanical performance of styrene butadiene rubber/carbon black composites. J Leather Sci Eng 2024;6:7. https://doi.org/10.1186/s42825-024-00181-7.
[16] AZoM. Polybutadiene – properties, applications, processing and types of polybutadiene (BR) [Internet]. AZoM; 2013 [cited 2025 Oct 10]. Available from: https://www.azom.com/properties.aspx?ArticleID=1719.
[17] Alnafessah A, Al-Hammadi Y, Alzahrani A, Alzahrani B, Alotaibi R. Artificial neural networks-based techniques for anomaly detection. Clust Comput 2020;23:1781–96. https://doi.org/10.1007/s10586-019-02998-y.
[18] Hassan M, Ahmed N, Afzal H, Mehmood Z. Towards a deep learning-based outlier detection approach in the context of streaming data. J Big Data 2022;9:57. https://doi.org/10.1186/s40537-022-00670-8.
[19] Haykin S. Neural networks: a comprehensive foundation. second ed. New York: Prentice-Hall; 1995. ISBN: 978-0132733502.
[20] Russell S, Norvig P. Artificial intelligence: a modern approach. third ed. Upper Saddle River, NJ: Prentice Hall; 2010. ISBN: 978-0-13-604259-4.
[21] Rumelhart D, Hinton G, Williams R. Learning representations by back-propagating errors. Nature 1986;323:533–6. https://doi.org/10.1038/323533a0.
[22] Meireles MR, Almeida PE, Simões MG. A comprehensive review for industrial applicability of artificial neural networks. IEEE Trans Ind Electron 2003;50(3):484–601. https://doi.org/10.1109/TIE.2003.812470.
[23] Řeháčková L, Novák V, Rosypalová S, Heger M, Zimný O, Matýsek D, et al. On rheological properties of environmentally friendly inorganic systems and their modeling by artificial neural networks. J Mater Res Technol 2023;22:1410–22. https://doi.org/10.1016/j.jmrt.2022.12.014.

[24] Xiang KL, Xiang PY, Wu YP. Prediction of the fatigue life of natural rubber composites by artificial neural network approaches. Mater Des 2014;57:180–5. https://doi.org/10.1016/j.matdes.2013.12.044.
[25] Zhao S, Ma Y, Leng D. An intelligent artificial neural network modeling of a magnetorheological elastomer isolator. Algorithms 2019;12(9):195. https://doi.org/10.3390/a12090195.
[26] ASTM D3182-21a. Standard practice for rubber – materials, equipment, and procedures for mixing standard compounds and preparing standard vulcanized sheets. West Conshohocken, PA: ASTM International; 2007. Available from: https://compass.astm.org/document/?contentCode=ASTM%7CD3182-21A%7Cen-US.
[27] ASTM D412-16 (2021). Standard test methods for vulcanized rubber and thermoplastic elastomers – tension. West Conshohocken, PA: ASTM International; 2021. Available from: https://compass.astm.org/document/?contentCode=ASTM%7CD0412-16R21%7Cen-US.
[28] ASTM D624-00 (2020). Standard test method for tear strength of conventional vulcanized rubber and thermoplastic elastomers. West Conshohocken, PA: ASTM International; 2020. Available from: https://compass.astm.org/document/?contentCode=ASTM%7CD0624-00R20%7Cen-US.
[29] ASTM D2084-19a. Standard test method for rubber property – vulcanization using oscillating disk cure meter. West Conshohocken, PA: ASTM International; 2019. Available from: https://compass.astm.org/document/?contentCode=ASTM%7CD2084-19A%7Cen-US.
[30] Lee BL. Reinforcement of uncured and cured rubber composites and its relationship to dispersive mixing - an interpretation of cure meter rheographs of carbon black loaded SBR and cis-polybutadiene compounds. Rubber Chem Technol 1979;52(5):1019–29. https://doi.org/10.5254/1.3535250.
[31] ASTM D297-21. Standard test methods for rubber products – chemical analysis. West Conshohocken, PA: ASTM International; 2021. Available from: https://compass.astm.org/document/?contentCode=ASTM%7CD0297-21%7Cen-US.
[32] Todorova N, et al. Zinc resinate's influence on the properties of silica filled composites based on natural rubber. J Chem Technol Metall 2014;49(3):213–9. Available from: https://www.researchgate.net/publication/280774526_Zinc_resinate's_influence_on_the_properties_of_silica_filled_composites_based_on_natural_rubber.
[33] Mazorca AJ, Garraza ALR, Mansilla MA. Evaluation of the polymer–solvent interaction parameter χ for the system cured polybutadiene rubber and toluene. Polym Test 2010;29:119–26. https://doi.org/10.1016/j.polymertesting.2009.09.013.
[34] ASTM D2240-15 (2021). Standard test method for rubber property – durometer hardness. West Conshohocken, PA: ASTM International; 2021. Available from: https://compass.astm.org/document/?contentCode=ASTM%7CD2240-15R21%7Cen-US.
[35] Fröhlich J, Niedermeier W, Luginsland H-D. The effect of filler–filler and filler–elastomer interaction on rubber reinforcement. Compos Part A Appl Sci Manuf 2005;36(4):449–60. https://doi.org/10.1016/j.compositesa.2004.10.004.
[36] ASTM 5963-22. Standard test method for rubber property – abrasion resistance (rotary drum abrader). West Conshohocken, PA: ASTM International; 2022. Available from: https://compass.astm.org/document/?contentCode=ASTM%7CD5963-22%7Cen-US.
[37] Aggarwal CC. Neural networks and deep learning: a textbook. Cham: Springer; 2018. https://doi.org/10.1007/978-3-319-94463-0.
[38] Goodfellow I, Bengio Y, Courville A. Deep learning. Cambridge, MA: MIT Press; 2016.
[39] Bishop CM. Neural networks for pattern recognition. Oxford: Oxford University Press; 1995. https://doi.org/10.1093/oso/9780198538493.001.0001.
[40] Kayri M. Predictive abilities of Bayesian Regularization and Levenberg–Marquardt algorithms in artificial neural networks: a comparative empirical study on social data. Math Comput Appl 2016;21:20. https://doi.org/10.3390/mca21020020.
[41] The MathWorks Inc. MATLAB R2024b documentation. 2024. Available from: https://www.mathworks.com/help/index.html?s_tid=CRUX_lftnav.
[42] Kopal I, Harničárová M, Valíček J, Krmela J, Lukáč O. Radial basis function neural network-based modeling of the dynamic thermo-mechanical response and damping behavior of thermoplastic elastomer systems. Polymers 2019;11(6):1074. https://doi.org/10.3390/polym11061074.
[43] Vendittoli V, Polini W, Walter MSJ, Geißelsöder S. Using Bayesian regularized artificial neural networks to predict the tensile strength of additively manufactured polylactic acid parts. Appl Sci 2024;14(8):3184. https://doi.org/10.3390/app14083184.
[44] Madhiarasan M, Louzazni M. Analysis of artificial neural network: architecture, types, and forecasting applications. J Electr Comput Eng 2022;2022:5416722. https://doi.org/10.1155/2022/5416722.
[45] Padmavathi G, Mandan MG, Mitra SP, Chaudhuri KK. Neural modelling of Mooney viscosity of polybutadiene rubber. Comput Chem Eng 2005;29(7):1677–85. https://doi.org/10.1016/j.compchemeng.2005.02.028.
[46] Abdollahzadeh A, Mukhlisin M, El Shafie A. Predict soil erosion with artificial neural network in Tanakami (Japan). WSEAS Trans Comput 2011;10(2):51–60. Available from: https://www.researchgate.net/profile/Muhammad-Mukhlisin/publication/262393610_Predict_soil_erosion_with_artificial_neural_network_in_Tanakami_Japan/links/55cb063908aea2d9bdcc1538/Predict-soil-erosion-with-artificial-neural-network-in-Tanakami-Japan.pdf.
[47] Almaliki S, Alimardani R, Omid M. Artificial neural network based modeling of tractor performance at different field conditions. CIGR J 2016;18(4):262–74. Available from: https://cigrjournal.org/index.php/Ejounral/article/view/3880.
[48] Rezazadeh Eidgahee D, Haddad A, Naderpour H. Evaluation of shear strength parameters of granulated waste rubber using artificial neural networks and group method of data handling. Sci Iran 2019;26(6):3233–44. https://doi.org/10.24200/sci.2018.5663.1408.
[49] Onoji SE, Iyuke SE, Igbafe AI, Daramola MO. Hevea brasiliensis (rubber seed) oil: modeling and optimization of extraction process parameters using response surface methodology and artificial neural network techniques. Biofuels 2019;10(6):677–91. https://doi.org/10.1080/17597269.2017.1338122.
[50] Abdelkareem MA, Soudan B, Mahmoud MS, Sayed ET, Almallahi MN, Inayat A, Radi MA, Olabi AG. Progress of artificial neural networks applications in hydrogen production. Chem Eng Res Des 2022;182:66–86. https://doi.org/10.1016/j.cherd.2022.03.030.
[51] Abdelsalam AA, Araby S, El-Sabbagh SH, Abdelmoneim A, Hassan MA. Effect of carbon black loading on mechanical and rheological properties of natural rubber/styrene-butadiene rubber/nitrile butadiene rubber blends. J Thermoplast Compos Mater 2019;34(4):490–507. https://doi.org/10.1177/0892705719844556.
[52] Wetchakama P, Sriwongruang D, Sae-Oui P, Siriwong C. Characterization and utilization of cacao shell powder as a biofiller in natural rubber composite. J Mater Res Technol 2024;30:9130–9. https://doi.org/10.1016/j.jmrt.2024.06.005.
[53] Ahmed NM, El-Sabbagh SH. The influence of kaolin and calcined kaolin on SBR composite properties. Polymer Compos 2014;35(3):37–43. https://doi.org/10.1002/pc.22697.
[54] Dijkhuis KAJ, Noordermeer JWM, Dierkes WK. The relationship between crosslink system, network structure and material properties of carbon black reinforced EPDM. Eur Polym J 2009;45(11):3302–12. https://doi.org/10.1016/j.eurpolymj.2009.06.029.
[55] Kim DY, Park JW, Lee DY, Seo KH. Correlation between the crosslink characteristics and mechanical properties of natural rubber compound via accelerators and reinforcement. Polymers 2020;12:2020. https://doi.org/10.3390/polym12092020.
[56] Cruz MAG, Hiranobe CT, Cardim GP, Cabrera FC, Ribeiro GD, Tolosa GR, Garcia RE, dos Santos RJ. Artificial neural network modeling for predicting the carbon black content derived from unserviceable tires for elastomeric composite production. J Appl Polym Sci 2024;141(37):e55951. https://doi.org/10.1002/app.55951.
[57] Ribeiro GD, Hiranobe CT, Araújo SS, Filgueira MS, Job AE, Santos RJ, et al. Sustainable construction materials for low-cost housing: thermal insulation potential of expanded SBR composites with leather waste. J Mater Res Technol 2024;30:5590–604. https://doi.org/10.1016/j.jmrt.2024.04.234.
[58] Phomrak S, Nimpaiboon A, Newby BMZ, et al. Natural rubber latex foam reinforced with micro- and nanofibrillated cellulose via dunlop method. Polymers 2020;12:1959. https://doi.org/10.3390/polym12091959.
[59] Fei Z, Long C, Qingyan P, Shugao Z. Influence of carbon black on crosslink density of natural rubber. J Macromol Sci B 2012;51(6):1208–17. https://doi.org/10.1080/00222348.2012.664494.
[60] Dwivedi C, Manjare S, Rajan SK. Recycling of waste tire by pyrolysis to recover carbon black: alternative & environment-friendly reinforcing filler for natural rubber compounds. Compos Part B Eng 2020;200. https://doi.org/10.1016/j.compositesb.2020.108346.
[61] Norris CJ, López Cerdán A, Ter Haar P. Understanding recovered carbon black. Rubber Chem Technol 2023;96(2):196–213. https://doi.org/10.5254/rct.23.76956.